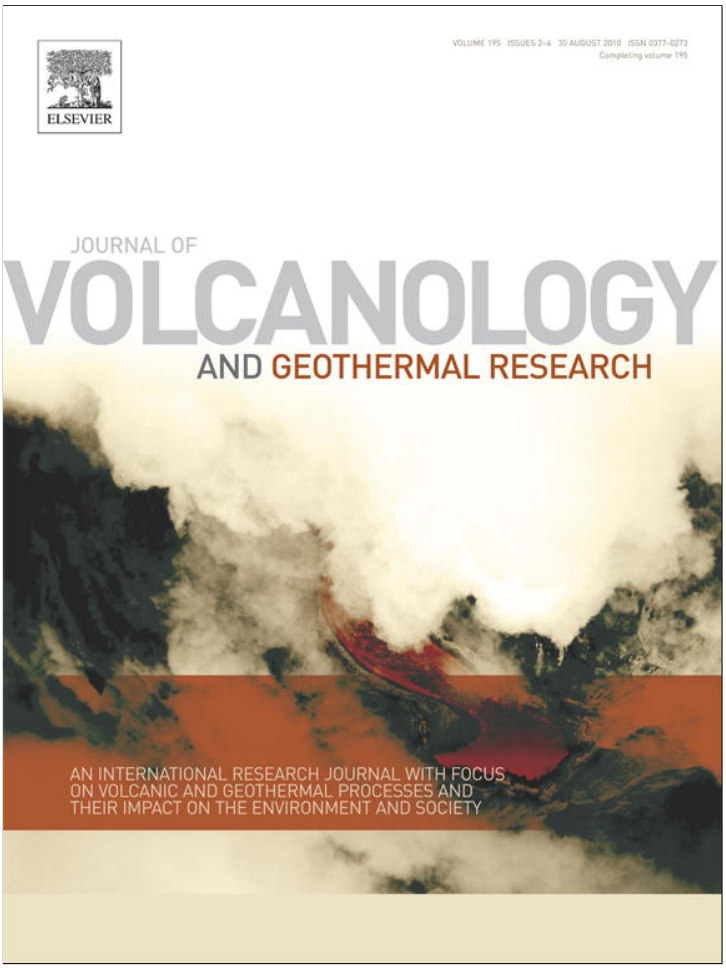

Journal of Volcanology and Geothermal Research 195 (2010) 97–105

Contents lists available at ScienceDirect

Journal of Volcanology and Geothermal Research

journal homepage: www.elsevier.com/locate/jvolgeores

The limitations of melting on the reactivation of silicic mushes

Christian Huber [a,*], Olivier Bachmann [b], Josef Dufek [a]

[a] School of Earth and Atmospheric Sciences, Georgia Institute of Technology, Atlanta, United States
[b] Department of Earth and Space Sciences, University of Washington, Seattle, United States

ARTICLE INFO

Article history:
Received 29 January 2010
Accepted 11 June 2010
Available online 22 June 2010

Keywords:
magma chamber
mush
intrusion
melting
crystallinity

ABSTRACT

High crystallinity silicic ignimbrites (such as the Monotonous Intermediates) typically erupt magma with an average crystallinity ranging from 40 to 50%. This average crystallinity is believed to be just under the threshold at which magma behaves as a solid (50–60% crystals), i.e. the locking point crystallinity, where convection is suppressed and large eruptions are unlikely. These magmas often display textural features which suggest that their average crystallinity was once higher and decreased before the eruption as a result of reheating through the injection of new magma. In this study, we use a theoretical 1D heat conduction model with phase change to test the ability of different melting scenarios of crystal mushes to meet the 40 to 50% crystallinity constraint observed in the field. Our heat conduction and melting models allow us to derive analytical solutions for the average crystallinity in the magma body (initially a crystal mush). We focus on the propagation of the melting front coinciding with the locking point crystallinity for different crystallinity–temperature relationships and various choices of temperature boundary conditions. We develop another analytical model based on stagnant-lid convection scaling to assess the role of convection on the expected average crystallinity of the magma subjected to wholesale steady-state convection. We find that, for all realistic melting scenarios, the average crystallinity of a silicic magma body that passed through the rheological transition is always substantially lower than what is observed in the field. We further show with a simple energy balance that the thermal energy needed to unlock/remobilize these magma bodies requires the intrusion of about an order of magnitude of more magma than the mush. Based on these results we argue that, although melting is a key process in the thermal reactivation of high crystallinity magma bodies, another coupled process is required in order to reactivate large volumes of crystal mushes. Moreover this additional process has to (1) be more efficient energetically and (2) lead to a smaller overall crystallinity reduction than melting alone.

1. Introduction

Magmas spend most of their suprasolidus lifespan at high crystallinity. Crystal-rich magmas (mushes) have a low thermal contrast with the surrounding crust and latent heat buffering is expected to significantly decrease the cooling rate as magma approach the solidus (Marsh, 1981; Koyaguchi and Kaneko, 1999, 2001; Huber et al., 2009). Upon injection of new magma at the base of a rheologically locked crystal mush, heat transfer and injection of exsolved volatiles from the intrusion can partially melt the base of the mush, decreasing its crystallinity below the locking point (Couch et al., 2001; Bachmann and Bergantz, 2006). Partial melting leading to wholesale convective stirring of large crystal mushes induced by the heat transfer of repeated intrusions of more mafic magma has been invoked as the process that can explain (1) the homogeneity of crystal-rich ignimbrites at the hand sample scale and (2) the ubiquitous chemical zoning and complex textures displayed by the mineral phases (Hildreth, 1981; Lindsay et al., 2001; Bachmann and Dungan, 2002; Bachmann and Bergantz, 2004; Christiansen, 2005; Ruprecht et al., 2008; Huber et al., 2009).

Magma chamber processes have to be reconstructed from few available constraints obtained from petrological observations. The most frequently used constraint to discern between different scenarios is the time available for dynamic processes to occur. It is usually inferred from field and stratigraphic observations, as well as from timescales obtained using geochronology and mineral–melt disequilibrium (Turner and Costa, 2007; Costa, 2008). Yet another more restrictive constraint is readily available but has rarely been the focus of any study: the average crystallinity of the erupted products. What physical process (or combination of physical processes) melts and mixes a locked-up crystal mush with about 50–65% crystals to an homogeneous magma mixture with a crystallinity 40–50%? It is generally assumed that, at the low strain-rates expected in crystal-rich silicic magmas, magma behaves as a rigid body at about 50% crystallinity (Marsh, 1981; Vigneresse et al., 1996; Petford, 2003). The observation of homogenous magma bodies erupting with a crystallinity of 40–50% (see Table 1) is therefore a difficult

* Corresponding author.
E-mail address: christian.huber@eas.gatech.edu (C. Huber).

0377-0273/$ – see front matter © 2010 Elsevier B.V. All rights reserved.
doi:10.1016/j.jvolgeores.2010.06.006

Table 1
Average crystallinity measured in examples of Monotonous Intermediates. Measurement of crystallinity in pyroclastic units need to be performed on pumice samples, but the typical small size of pumices and the presence of vesicles lead to some variability in the results. The units above are chosen as they provide possibly the most reliable estimates for Monotonous Intermediates.

Unit name	Location	Average crystallinity	References
Fish Canyon Tuff	San Juan Volcanic Field, Colorado	~45%	Bachmann et al. (2002)
Snowshoe Mtn Tuff	San Juan Volcanic Field, Colorado	~40%	Lipman (2004)
Blue Creek Tuff	San Juan Volcanic Field, Colorado	~40%	Lipman (2004)
Masonic Park Tuff	San Juan Volcanic Field, Colorado	~40%	Lipman (2004)
Lund Tuff	Great Basin, Utah	~45%	Maughan et al. (2002)
Cerro Galan ignimbrite	Central Andes	~45%	Folkes et al. (in press)
Atana ignimbrite	Central Andes	≥35–40%	Lindsay et al. (2001)

constraint to satisfy as it involves a limited crystallinity reduction (10–20% volume in most cases) just below the locking point and, moreover, that the crystallinity has to decrease everywhere below the locking point in the active magma body. For very large magma bodies like the Fish Canyon magma body, we show that this constraint is difficult to satisfy with standard melting models.

In this study, we use the state of the magma prior to the eruption as the major constraint to build a physical model to explain the reactivation of mushes. In the first section, we present a simplified 1D analytical model which does not include the heat transported by buoyant volatiles. This model takes into account phase change with a complex (i.e. non-linear) crystallinity–temperature relationship. The model allows us to track the propagation of the locking front, defined here as the fixed crystallinity set at the locking point threshold, during melting. The model enable us to calculate the final average crystallinity expected for the case where the heat transfer solely controls the rheological state of the mush. We show that melting alone cannot satisfy the final crystallinty constraint for most of the range of parameters expected in real systems. The average crystallinity reduction expected when the lock-up front reaches the roof of the magma chamber is generally greater than observed in the field. This can be explained by the substantial amount of melting that occurs in the lower region of the mush when the melting front reaches the top of the magma body. We also calculate the average crystallinity in a fully reactivated mush assuming a steady convection with different temperature–crystallinity relationships. We observe that in all cases the final average crystallinity is always much lower than what is observed in the field for crystal-rich silicic magmas. These results suggest that melting alone cannot be solely responsible for the high (40–50%) and homogenous crystallinity of Monotonous Intermediate magmas.

2. Melting model

The symbols used in the calculations are listed in Table 2. The conceptual model for the melting problem is shown in Fig. 1. The intrusion at the base heats up the lowermost part of the mush and opens it to sluggish convection. We discretize the physical domain into sections with boundaries set-up at fixed temperatures/crystallinities (therefore moving upwards at different pace as the mush melts). This, as we show later, allows us to deal with non-linear crystallinity–temperature relationships. In this study we use a power-law parameterization

$$\chi = 1-\phi = 1-\left(\frac{T-T_s}{T_l-T_s}\right)^b \qquad 0<b\leq 1, \tag{1}$$

Table 2
List of parameters and symbols.

Symbol	Description	Value	Units
b	Exponent relating temperature to crystallinity for mush	0.4 to 1	
$c_x = c$	Specific heat for phase x	1200	J/kg K
g	Acceleration due to gravity		m^2
H	Mush thickness	2000	m
H_l	Thickness of Unlocked layer		m
$\mathcal{H}$	Intrusion thickness		m
k	Thermal conductivity	$\kappa\rho_m c$	W/m K
L	Latent heat of crystallization (intrusion/mush)	300	kJ /kg
Q	Activation energy for dynamic viscosity	500	kJ
R	Ideal gas constant	8.314	J/K mol
S	Stefan number (latent/sensible heat)	1	
T_b	Intrusion–mush interface temperature		°C
T_{ini}	Initial temperature of intrusion	895	°C
T_{lock}	Locking point temperature (depends on b)		°C
T_l	Mush liquidus temperature	1000	°C
T_s	Mush solidus temperature	700	°C
ΔT_e	Temperature difference driving convection in the intrusion		°C
α_T	Thermal expansion coefficient	3×10^{-5}	1/T
δ_i	Boundary layer thicknesses		m
$\chi = 1-\phi$	Crystallinity of intrusion / mush		
χ_{cr}	Critical crystallinity	0.5	
ϕ	Melt fraction		
ϕ_{ini}	Initial melt fraction in the mush	0.45 or 0.35	
ϕ_l	Locking point melt fraction	0.5 or 0.4	
κ	Thermal diffusivity	10^{-6}	m^2/s
ρ_c	Density of the melt in the mush	2800	kg/m^3
ρ_m	Density of the melt in the mush	2600	kg/m^3
μ	Dynamic viscosity		Pa s

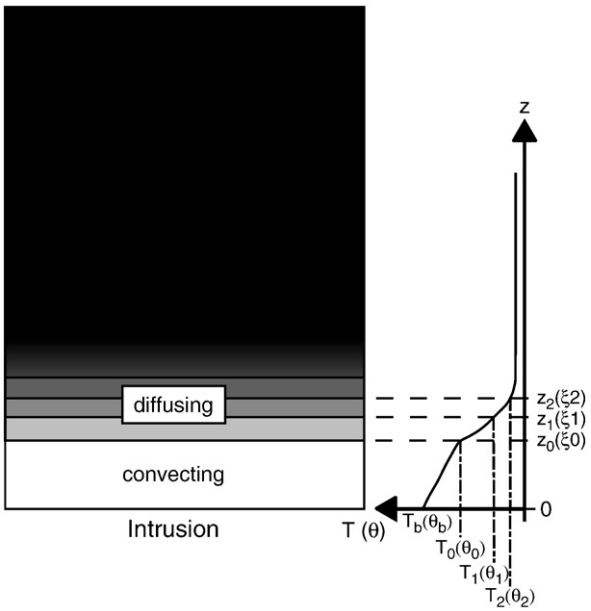

Fig. 1. Setup of the 1D conceptual model. The dimensionless or similarity variable used later in the development of the mathematical model is shown in parenthesis for reference. The physical domain is treated as a succession of N sections coupled through boundary conditions. This procedure allows us to solve for Eqs. (9) and (10) even for non-linear temperature–crystallinity relationship as expected from silicic magmas.

where χ is the crystallinity (ϕ the melt fraction), b is the power-law exponent, T_s, T_l are respectively the solidus and liquidus temperature of the mush. Silicic magmas with eutectic behavior tend to have low b values (about 0.4–0.5 for dacitic mush). As b decreases, the phase diagram becomes more non-linear with steeper slope near the solidus. The methodology we use here is inspired by Feltham and Worster (2000). The general heat equations are

$$(\rho_s c_s(1-\phi)+\rho_m c_m \phi)\frac{\partial T}{\partial t}=\frac{\partial}{\partial z}\left(k_{mix}\frac{\partial T}{\partial z}\right)-\rho_s L\frac{\partial \phi}{\partial t},\quad H_l(t)\le z, \tag{2}$$

in the mush regions and

$$(\rho_s c_s(1-\phi)+\rho_m c_m \phi)\frac{\partial T}{\partial t}+\bar{u}_z\frac{\partial T}{\partial z}=\frac{\partial}{\partial z}\left(k_{mix}\frac{\partial T}{\partial z}\right)-\rho_s L\frac{\partial \phi}{\partial t},\quad 0\le z\le H(t), \tag{3}$$

in the convecting part. $H_l(t)$ is the position of the interface between the convecting part and the rigid mush (controlled by the position where the melt fraction $\phi=\phi_l\approx 0.5$). The subscripts s and m refer respectively to the solid and melt fractions, c is the specific heat, ρ the density, $\bar{u}_z$ the average advective flux in the convecting region ($\bar{u}_z=c\rho u$), L the latent heat of fusion and k_m the thermal conductivity of the solid–melt mixture. The generalized heat flux in the convecting part is

$$J_h=\bar{u}_z\Delta T-k_{mix}\frac{\partial T}{\partial z}. \tag{4}$$

We will simplify the treatment by neglecting the advection term in order to find analytical solutions and assume the physical properties of the melt and solid to be similar $\rho_s=\rho_m=\rho$, $c_s=c_m=c$ and $k_{mix}=k$. Using $\theta=(T-T_s)/(T_l-T_s)$, and using the following time κ/V^2 and spatial scales κ/V, where $\kappa=k/(\rho c)$ and V is a characteristic velocity scale, Eqs. (2) and (3) become

$$\frac{\partial \theta}{\partial t*}=\frac{\partial^2\theta}{\partial z^{*2}}-S\frac{\partial \phi}{\partial t*} \tag{5}$$

where $S=L/(c\Delta T)$ is the Stefan number, which represents the ratio of sensible to latent heat, and superscript denotes dimensionless variables. Using Eq. (1), we can rewrite the heat equation in dimensionless form

$$\frac{\partial}{\partial t*}\left(\theta+S\theta^b\right)=\frac{\partial^2\theta}{\partial z^{*2}}. \tag{6}$$

We simplify the non-linear melt fraction–temperature relationship by discretizing the domain in segments of various length Δz^* with fixed temperature/melt fraction values at their boundaries. We will linearize $\phi(\theta)$ over these segments and extract from the model N heat equations coupled through their moving boundary conditions. The length of these segments depends on the non-linearity (exponent b) of the temperature–melt fraction relationship. The size of each segment in θ space is obtained by satisfying the following condition

$$\left|\frac{d\phi}{d\theta}\right|\Delta\theta=\frac{c_1}{2}\left|\frac{d^2\phi}{d\theta^2}\right|(\Delta\theta)^2, \tag{7}$$

where c_1 is a constant (greater than 1) that ensures that the segment is short enough that second order terms in the Taylor series expansion can be neglected. From this condition we can set-up appropriate temperature boundary conditions that depend on the non-linearity of $\phi(T)$

$$\Delta\theta_i=\theta_i-\theta_{i-1}=\frac{2}{c_1(1-b)}\theta_i. \tag{8}$$

We introduce the similarity variable $\eta=zt^{-1/2}$ and assume that the position of boundaries between segments move according to $\xi_i=\lambda_i t^{*1/2}$ and therefore are positioned at constant $\eta_i=\xi_i$ (see Fig. 1).

Owing to a stronger non-linear behavior of ϕ near solidus conditions, we will further assume that ϕ is linear over the whole region opened to convection. In terms of η the N heat equations become

$$-\frac{\eta}{2}\Omega\frac{d\theta}{d\eta}=\frac{d^2\theta}{d\eta^2}\quad 0\le\eta\le\xi_0, \tag{9}$$

and $N-1$ segments in the locked-up mush

$$-\frac{\eta}{2}\Omega\frac{d\theta}{d\eta}=\frac{d^2\theta}{d\eta^2}\quad \xi_i\le\eta\le\xi_i+1,\quad i=0,\ldots,N-100; \tag{10}$$

where we introduced $\Omega=(1+S)$. The boundary conditions are

$$\theta(0)=\theta_b \tag{11}$$

$$\theta(\lambda_0)=\theta_{lock}=\phi_l^{1/b} \tag{12}$$

$$\theta(\lambda_i)=\theta_i\quad i=1,\ldots,N-1 \tag{13}$$

$$\theta(\infty)=\theta_\infty \tag{14}$$

where ϕ_l is the melt fraction at the rheological transition, θ_b is the temperature of the intrusion and the top boundary condition is assumed to be at a fixed temperature in the far field. The latter boundary condition is not ideal in our case and we will assume that the solution of the thermal problem will only be affected by this assumption near the top boundary condition. A justification of this assumption resides in the fact that, owing to the phase diagram of the mush, the thermal front beyond the interface between convecting and locked-up mush is restricted to a narrow region because of the low thermal diffusivity and the presence of melting. It will therefore contribute to relatively minor errors in the calculation of the average crystallinity over a large chamber (if the chamber thickness is much greater than the region of strong thermal gradients near the locking

point). Another set of boundary conditions comes from matching the heat fluxes on each side of each interface

$$\left(\frac{d\theta}{d\eta}\right)_{\lambda_0^-} = \left(\frac{d\theta}{d\eta}\right)_{\lambda_0^+} \tag{15}$$

$$\left(\frac{d\theta}{d\eta}\right)_{\lambda_i^-} = \left(\frac{d\theta}{d\eta}\right)_{\lambda_i^+} \quad i = 1,\ldots,N-1, \tag{16}$$

where the subscripts λ_i^- and λ_i^+ refer to the positions just below and above the interface λ_i.

The solutions to Eqs. (9) and (10) are given by

$$\theta(\eta) = \frac{\theta_{lock}-\theta_b}{erf\left(\frac{\Omega^{1/2}\lambda_0}{2}\right)} erf\left(\frac{\Omega^{1/2}\eta}{2}\right) + \theta_b, \quad 0 \le \eta \le \lambda_0, \tag{17}$$

$$\theta(\eta) = \frac{\theta_i-\theta_{i-1}}{erf\left(\frac{\Omega^{1/2}\lambda_i}{2}\right)-erf\left(\frac{\Omega^{1/2}\lambda_{i-1}}{2}\right)}\left[erf\left(\frac{\Omega^{1/2}\eta}{2}\right)-erf\left(\frac{\Omega^{1/2}\lambda_{i-1}}{2}\right)\right] + \theta_{i-1}, \quad \lambda i-1 \le \eta \le \lambda_i, \quad i = 1,\ldots,N-1 \tag{18}$$

and finally

$$\theta(\eta) = \frac{\theta_\infty-\theta_{N-1}}{erfc\left(\frac{\Omega^{1/2}\lambda_{N-1}}{2}\right)}\left[erf\left(\frac{\Omega^{1/2}\eta}{2}\right)-erf\left(\frac{\Omega^{1/2}\lambda_{N-1}}{2}\right)\right] + \theta_{N-1}, \quad \lambda N-1 \le \eta \le H. \tag{19}$$

To solve these equations requires determining the values of the constants λ_i $(i=0,\ldots,N-1)$. This is done by applying the flux boundary conditions to get

$$\left(\frac{\theta_{lock}-\theta_b}{\theta_1-\theta_{lock}}\right) = \frac{erf\left(\frac{\Omega^{1/2}\lambda_0}{2}\right)}{erf\left(\frac{\Omega^{1/2}\lambda_1}{2}\right)-erf\left(\frac{\Omega^{1/2}\lambda_0}{2}\right)}, \tag{20}$$

$$\left(\frac{\theta_i-\theta_{i-1}}{\theta_{i+1}-\theta_i}\right) = \frac{erf\left(\frac{\Omega^{1/2}\lambda_i}{2}\right)-erf\left(\frac{\Omega^{1/2}\lambda_{i-1}}{2}\right)}{erf\left(\frac{\Omega^{1/2}\lambda_{i+1}}{2}\right)-erf\left(\frac{\Omega^{1/2}\lambda_i}{2}\right)}, \quad i = 1,\ldots,N-2, \tag{21}$$

and

$$\left(\frac{\theta_{N-1}-\theta_{N-2}}{\theta_\infty-\theta_{N-1}}\right) = \frac{erf\left(\frac{\Omega^{1/2}\lambda_{N-1}}{2}\right)-erf\left(\frac{\Omega^{1/2}\lambda_{N-2}}{2}\right)}{erfc\left(\frac{\Omega^{1/2}\lambda_{N-1}}{2}\right)}. \tag{22}$$

These coupled equations then need to be solved to obtain the values of the λs and especially λ_0 which will allow us to compute the temperature and melt fraction profiles at the time when the unlocking front reaches the top of the mush at $z=H$, the time is given by

$$\tau = \frac{H^2}{\kappa\lambda_0^2}, \tag{23}$$

where H is the thickness of the mush. Setting $\eta = z/(\kappa\tau)^{1/2}$ in Eq. (17), we can compute the temperature profile and therefore obtain the average crystallinity at the time the system is fully reactivated. The average crystallinity is obtained with

$$\langle\chi\rangle = 1-\frac{1}{\lambda_0}\int_0^{\lambda_0}\theta(\eta)^b d\eta. \tag{24}$$

2.1. The effect of convection

Large crystal mushes start to convect when melting unlocks a region thicker than the critical boundary layer thickness (Turcotte and Schubert, 2002). The critical boundary layer thickness is controlled by the rheology of the crystal–melt mixture and the crystallinity–temperature relationship of the mush. In order to compare the results obtained with the analytical model for heat conduction presented above and the results expected when accounting for convective heat fluxes, we use a simplified model, where we focus on the temperature profile expected from steady-state convection in a fully reactivated mush with a temperature and crystallinity-dependent viscosity. We use empirical and scaling results obtained from stagnant-lid convection (Davaille and Jaupart, 1993). Fig. 2 illustrates schematically the temperature profile expected for steady (or time-averaged) convection once the locking point has reached the top of the mush.

For simplicity we assume that the temperature profiles are linear in segments between θ_b and θ_1, θ_1 and θ_2 and θ_2 and θ_{lock}. We also assume that the temperature difference driving the convection $\theta_1-\theta_2$ is comparable to the viscous temperature scale ΔT_v (Davaille and Jaupart, 1993)

$$T_1-T_2 = (T_l-T_s)(\theta_1-\theta_2) = \Delta T_e, \tag{25}$$

and

$$\Delta T_e \approx 2\Delta T_v = -2\frac{\mu(T_m)}{\frac{d\mu}{dT}(T_m)}, \tag{26}$$

where T_m is roughly the average temperature in the convecting part $(T_2<T_m<T_1)$. We use a temperature and crystallinity-dependent viscosity (Dingwell et al., 1993)

$$\mu(T) = \mu_0 \exp\left[\frac{Q}{RT_{ini}}\left(\frac{T_{ini}}{T}-1\right)\right]\left[1+0.75\frac{\chi(T)/\chi_{cr}}{1-\chi(T)/\chi_{cr}}\right]^2 \tag{27}$$

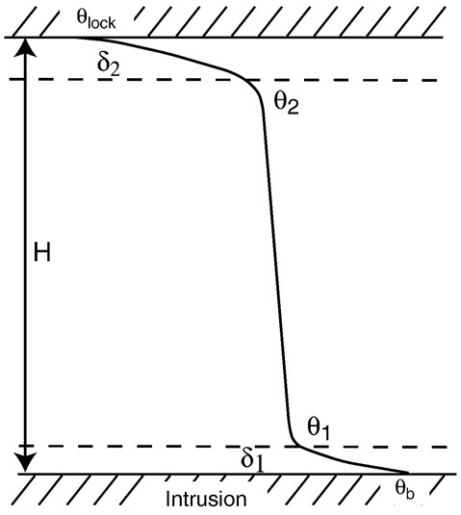

Fig. 2. Schematic temperature profile in the reactivated mush subjected to whole-scale steady-state convection.

where Q is the activation energy (fixed here at 500 kJ/mol), R is the ideal gas constant, T_{ini} is the reference temperature (consistent with μ_0) and χ_{cr} is the critical crystallinity at which the magma behaves like a solid. The symbols and the values used in the calculations are listed in Table 1.

Matching heat fluxes at steady-state and assuming a constant thermal conductivity in the mush (same assumption as for the conduction model), we obtain

$$T_1 = \frac{T_b\delta_1 + \delta_2(T_{lock} + \Delta T_e)}{\delta_1 + \delta_2} \tag{28}$$

and

$$T_2 = \frac{T_b\delta_1 + \delta_2 T_{lock} - \delta_1\Delta T_e}{\delta_1 + \delta_2}, \tag{29}$$

where δ_1 and δ_2 are respectively the lower and upper boundary layers. The upper boundary layer thickness is controlled by the viscous temperature scale ΔT_v and can be estimated with the scaling of (Davaille and Jaupart, 1993) for stagnant-lid convection cooled from the top

$$\delta_2 = \frac{1}{C}\left[\frac{\Delta T_m}{\Delta T_v} - \frac{\Delta T_e}{\Delta T_v}\right]\left(\frac{\alpha g \Delta T_v}{\kappa \nu_m}\right)^{-1/3}, \tag{30}$$

where $C = 0.47$ is determined experimentally (Davaille and Jaupart, 1993), κ is the thermal diffusivity and ν_m is the kinematic viscosity at $T = T_m$. The buoyancy effect of crystallinity variations is introduced in α

$$\alpha = -\frac{\rho_c - \rho_m}{\rho_0}\frac{\partial\phi}{\partial T} + \alpha_T, \tag{31}$$

where α_T is the thermal expansion coefficient (about 3×10^{-5} 1/K), ρ_c and ρ_m are the density of the crystals and melt phases.

The lower boundary layer thickness δ_1 is determined by matching heat fluxes

$$\delta_1 = \frac{T_b - T_1}{C\left(\frac{\alpha g}{\kappa\nu_m}\right)^{1/3}\Delta T_v^{4/3}}. \tag{32}$$

The upper boundary layer thickness δ_2 depends only on the rheology and crystallinity–temperature relationships of the magma once the temperature difference driving convection is greater than the viscous temperature scale. It is therefore calculated first. The lower boundary layer thickness δ_1 is then calculated from Eqs. (28), (29) and (32)

$$\delta_1 = \frac{A\Delta T_e - \delta_2 + \sqrt{(A\Delta T_e - \delta_2)^2 + 4A(T_b - T_{lock})\delta_2}}{2}, \tag{33}$$

where

$$A = \frac{1}{C\left(\frac{\alpha g}{\kappa\nu_m}\right)^{1/3}\Delta T_v^{4/3}}. \tag{34}$$

The average crystallinity is then obtained with

$$\langle\chi\rangle = \frac{1}{H}\int_0^H \left[1 - \left(\frac{T(z) - T_s}{T_l - T_s}\right)^b\right]dz, \tag{35}$$

and

$$T(z) = \begin{cases} T_b - (T_b - T_1)\dfrac{z}{\delta_1} & \text{if } 0 \le z \le \delta_1 \\ T_1 - (T_1 - T_2)\dfrac{z - \delta_1}{H - \delta_1 - \delta_2} & \text{if } \delta_1 \le z \le H - \delta_2 \\ T_2 - (T_2 - T_{lock})\dfrac{z - (H - \delta_2)}{\delta_2} & \text{if } H - \delta_2 \le z \le H. \end{cases} \tag{36}$$

Integrating Eq. (36) leads to

$$\begin{aligned}\langle\chi\rangle = 1 &+ \frac{\delta_1}{H(b+1)}\left(\frac{T_l - T_s}{T_b - T_1}\right)\left[\left(\frac{T_1 - T_s}{T_l - T_s}\right)^{b+1} - \left(\frac{T_b - T_s}{T_l - T_s}\right)^{b+1}\right] \\ &+ \frac{H - \delta_1 - \delta_2}{H(b+1)}\left(\frac{T_l - T_s}{T_1 - T_2}\right)\left[\left(\frac{T_2 - T_s}{T_l - T_s}\right)^{b+1} - \left(\frac{T_1 - T_s}{T_l - T_s}\right)^{b+1}\right] \\ &+ \frac{\delta_2}{H(b+1)}\left(\frac{T_l - T_s}{T_2 - T_{lock}}\right)\left[\left(\frac{T_{lock} - T_s}{T_l - T_s}\right)^{b+1} - \left(\frac{T_2 - T_s}{T_l - T_s}\right)^{b+1}\right].\end{aligned} \tag{37}$$

The average crystallinity for the convective case therefore depends principally on the viscous temperature scale ΔT_v and ultimately on the choice of crystallinity–temperature relationship (the power-law exponent b).

Eqs. (20)–(22) are solved numerically to obtain the N λs. We use Eqs. (20) and (21) to solve for λ_i, $i = 1,\ldots,N-1$, assuming different values for λ_0. We then compute a residual between the value obtained for λ_{N-1} from Eqs. (21) and (22). The value of λ_0 that minimizes the residual is then used to compute the average crystallinity of a mush fully opened to convection with Eqs. (24) and (17). We compute the final average crystallinity for a range of temperature–crystallinity power-law exponents $b \in [0.4:1]$ and intrusion–mush temperature boundary condition $\theta_b \in [0.5:0.85]$.

3. Results

Results presented in this paper focus on the post-reheating average crystallinity of the magma and compare it with the observation of homogeneous crystal content of Monotonous Intermediates. Fig. 4(a) shows the average crystallinity of the reactivated mush (once the 50% crystallinity front has been pushed to the top) as function of the intrusion temperature θ_b and the crystallinity–temperature power-law exponent b. We emphasize that, owing to the self-similar nature of the temperature profile obtained in Eq. (17), the results are independent of the mush thickness. However, 1D approximation still requires that the width of the mush is substantially greater than its thickness.

The average crystallinity found for a range of power-law exponents b (from 1 to 0.4; i.e., from andesite to dacite) and for a range of ΔT between the mush and the intrusion is typically lower than the 40–50% found in erupted crystal-rich ignimbrites (Fig. 4(a–b)). Fig. 4(a) shows that for a fixed intrusion–mush boundary condition temperature $\theta_b = 0.6$, the average crystallinity inferred from the conduction model is a strong function of the power-law exponent. Melting of crystal mushes with a higher power-law exponent b (closer to linear temperature–crystallinity relationship) leads to a final average crystallinity that is close to what is observed for crystal-rich dacitic erupted magmas. However, as shown by Huber et al. (2009, 2010) (see Fig. 3), dacitic mushes are better described with exponents $b = 0.4 - 0.5$, i.e. where a greater part of the overall melting happens just above the solidus. For these low b values, the expected final average crystallinity of the reactivated mush is ranging between 0.3 and 0.38 depending on the value of intrusion–mush temperature boundary condition θ_b.

Results of pre-eruptive average crystallinity obtained with the convection model for a 2 km thick magma body illustrate the importance of (1) the boundary temperature between the two magmas (θ_b) and (2) the power-law exponent for the crystallinty–temperature relationship

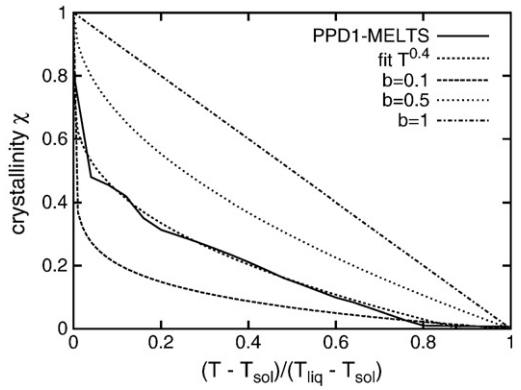

Fig. 3. Crystallinity–temperature relationships for the mush from Eq. (1) for different values of *b*. As *b* decreases towards 0, the system tends to melt more just above the solidus temperature. The crystallinity–temperature relation for the Fish Canyon magma body (dacite) calculated with MELTS (Ghiorso and Sack, 1995) is shown as a reference. The Fish Canyon magma is consistent with an exponent b~0.4.

(Fig. 4(b)). The boundary temperature controls the temperature and therefore the physical properties of the magma within the convecting layer, the crystallinity–temperature relationship controls the rheology of the magma and therefore the viscous temperature scale ΔT_v. For low *b* values, the average crystallinity expected from steady-state convection ranges from 0.22 to 0.29, significantly lower than crystallinities observed in the deposits.

4. Discussion

4.1. Final average crystallinity

Our calculations, summarized in Fig. 4, illustrate the difficulty of satisfying the 45% average crystallinity constraint for fully reactivated mushes when invoking only melting. The only conditions under which the final average crystallinity is close to the 40–50% crystallinity window observed in many large crystal-rich dacitic ignimbrites are consistent with much more mafic mush compositions ($b \rightarrow 1$). However, such reactivated andesitic crystal-rich units are yet to be found in the rock record (Hildreth, 1981; Christiansen, 2005; Bachmann and Bergantz, 2008). In addition, convection is expected to occur when parts of the mush become unlocked, and our results show that final average crystallinities are even lower in this case, as convection leads to a more efficient heat transfer between the intrusion and the mush.

The importance of *b* on the mush average crystallinity is logical. It controls the partitioning of enthalpy between sensible and latent heat and therefore the degree of melting expected for a given amount of heat injected in the mush. At small *b* values, melting is expected to become more important at temperatures close to the solidus and a greater portion of the heat flux is absorbed to reduce the crystallinity of the mush, leading to lower average crystallinity values.

An important assumption in our analytical model is that the temperature at the intrusion–mush boundary remains constant during the whole melting process. This assumption results in an overestimation of the heat transfer when compared to real cases where the thermal disequilibrium between the two magmas decreases as a result of the mush heating up and the intrusion cooling down. The interface temperature decreases with time as expected from conjugate heat transfer problems (Huber et al., 2010).

We deal with this assumption by calculating the expected variation of the average mush crystallinity as function of various fixed boundary condition temperature θ_b. The initial temperature difference $\theta_b - \theta_{lock}$ ranges from 0.05 to 0.4 which represent respectively a difference of temperature of 15 and 120 °C between the intrusion and the rheological locking point temperature (crystallinity of 0.5). We observe that for a mush close to its eutectic point (small b) the final crystallinities are underestimating what we observe in the field, even for cases where the intrusion temperature is very close to the temperature corresponding to the locking point. Realistic cooling temperature boundary evolution between the intrusion and the mush are expected to be consistent with, early on, a large difference between the temperature of the intrusion and the locking temperature (high θ_b) and decreasing θ_b values with time. Qualitatively, the calculations conducted at low θ_b values can be used to represent the late stage evolution between the two magmas, but probably underestimate the amount of melting early after the injection of the intrusion.

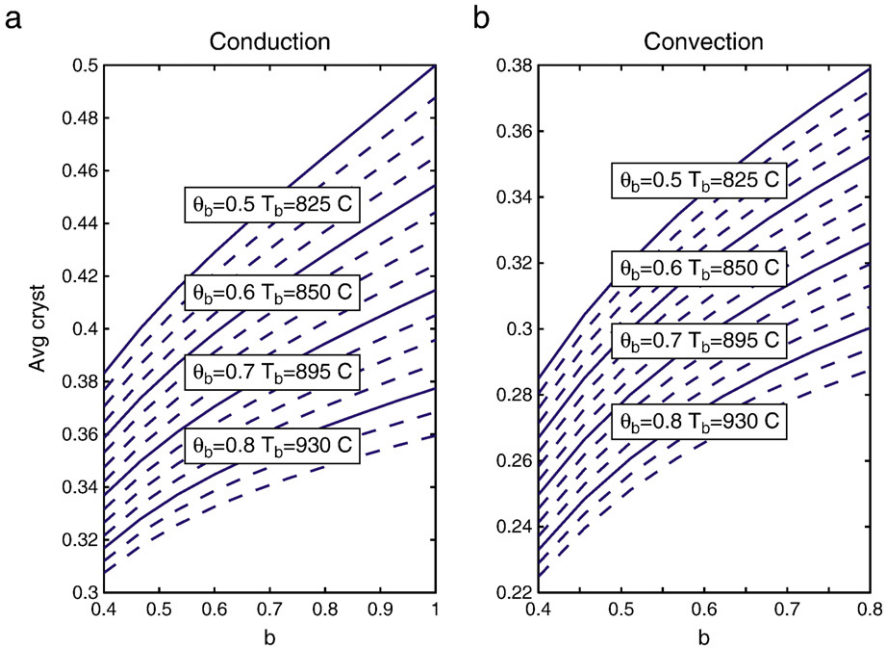

Fig. 4. Average crystallinities obtained with the analytical model for a locking point crystallinity of 0.5. The figure compares the conduction (a) and convection (b) models for various choices of temperature boundary conditions at the mush–intrusion interface (θ_b) and crystallinity–temperature power-law exponents (*b*).

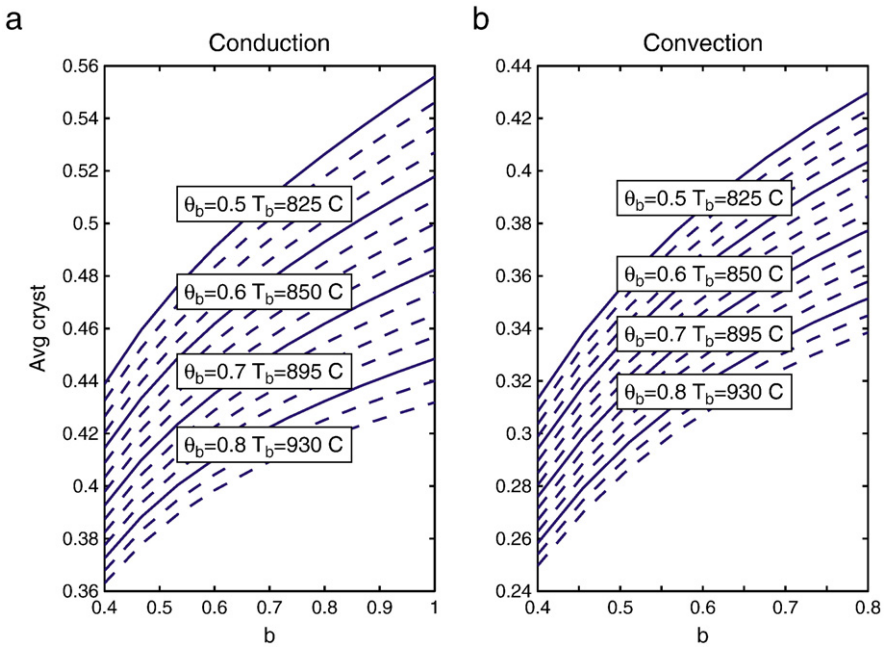

Fig. 5. Average crystallinities obtained with the analytical model for a locking point crystallinity of 0.6. The figure compares the conduction (a) and convection (b) models for various choices of temperature boundary conditions at the mush–intrusion interface (θ_b) and crystallinity–temperature power-law exponents (b).

Another poorly constrained parameter is the critical crystallinity at the rheological locking point which is usually assumed to be between 0.5 and 0.6. This threshold is usually determined from static percolation theory arguments and is expected to vary as a function of melt viscosity, suspended solid aspect ratios and applied stress. We show the sensitivity of the results with respect to the critical crystallinity in Fig. 5. If the crystallinity at the transition between a static rigid and a viscously deforming magma occurs at higher crystallinity (here, for example, $\chi_l = 1-\phi_l = 0.6$ and the initial mush crystallinity is set to 0.65), we observe, as expected, that the final average crystallinity is shifted to higher values. We note that under realistic circumstances, when the intrusion–mush temperature does not remain close to the locking temperature of the mush θ_{lock} for the whole duration of the melting event, the final crystallinity in our calculations usually underestimates field observations by at least 5 to 20%.

4.2. Energy requirements

Although the fixed temperature boundary condition between the mush and the intrusion implies that the intrusion is an infinite reservoir of heat, we can calculate the amount of energy that the intrusion has to provide to push the entire mush out of a locked-up state. This calculation allows us to assess the feasibility of the different melting scenarios. We will first assume that the heat transfer efficiency between the two magmas is 1, i.e. that all the heat lost by the intrusion is absorbed by the mush only. This assumption has been shown to be a very crude overestimate as thermal calculation usually result in to efficiency values of about 0.1 (Dufek and Bergantz, 2005). We calculate the thickness of intrusion H that is required to melt a mush of thickness H

$$R_h \equiv \frac{H}{H} = \frac{\int_0^H (c\Delta T + L\Delta\phi)dz}{H\left(c\Delta\,\bar{T} + L\Delta\,\bar{\phi}\right)}, \tag{38}$$

where the over bar refers to quantity averaged over the volume of the intrusion. We assumed the average specific heat c and latent heat L to be similar in both magmas, but use a different crystallinity–temperature relationship with $b=1$ for the intrusion and $b\in[0.4{:}1]$ for the mush. These calculations therefore correspond to the case where the intrusion is more mafic (andesitic) than the mush (dacite to andesite).

Fig. 6 shows the thickness ratio R_h for a lock-up crystallinity of 0.5. The amount of energy required by the intrusion to melt the mush depends strongly on the phase diagram of the mush (b). The enthalpy transferred from the intrusion is partitioned in sensible and latent heat in the mush. As our condition on the reactivation of the mush is based on the propagation of a melting front characterized by a critical crystallinity, the different melting scenarios calculated here require a comparable amount of heat absorbed by melting. However the amount of sensible heat absorbed by the mush depends on b. For a linear temperature–crystallinity relationship ($b=1$), the ratio of sensible to latent heat required to reduce the crystallinity by a given amount is constant between the solidus and the liquidus $R_{sl} = c(T_l - T_s)/L$. This is no longer true for $b<1$ where for a small given temperature shift from T_a to T_b

$$R_{sl} = \frac{c(T_b - T_a)}{L(\chi(T_a) - \chi(T_b))} \sim \frac{c\left(\frac{T_a - T_s}{T_l - T_s}\right)^{1-b}}{Lb}, \tag{39}$$

which illustrates that for $b<1$ and $T_a - T_s \ll T_l - T_s$, the ratio of sensible to latent heat that the mush needs to absorb gets smaller as b decreases. This, together with the assumption that the amount of enthalpy absorbed by melting is roughly similar in all cases, explains why the overall energy input required to reactivate a thermal mush increases with b. The last variable, the temperature of the intrusion θ_b, influences the amount of energy that a given volume of intrusion will be able to transfer to the mush. The size of the intrusion required by the simple energy balance statement of Eq. (38) decreases as θ_b increases.

The size of the intrusion varies roughly by one order of magnitude depending on the choice of b and θ_b for the conduction model. As previously mentioned, the simple balance of Eq. (38) assumes a perfect efficiency in the heat transfer between the two magmas, i.e. that all the energy lost by the intrusion is transferred to the mush. Most recent thermal calculations however show that the efficiency is about 10%

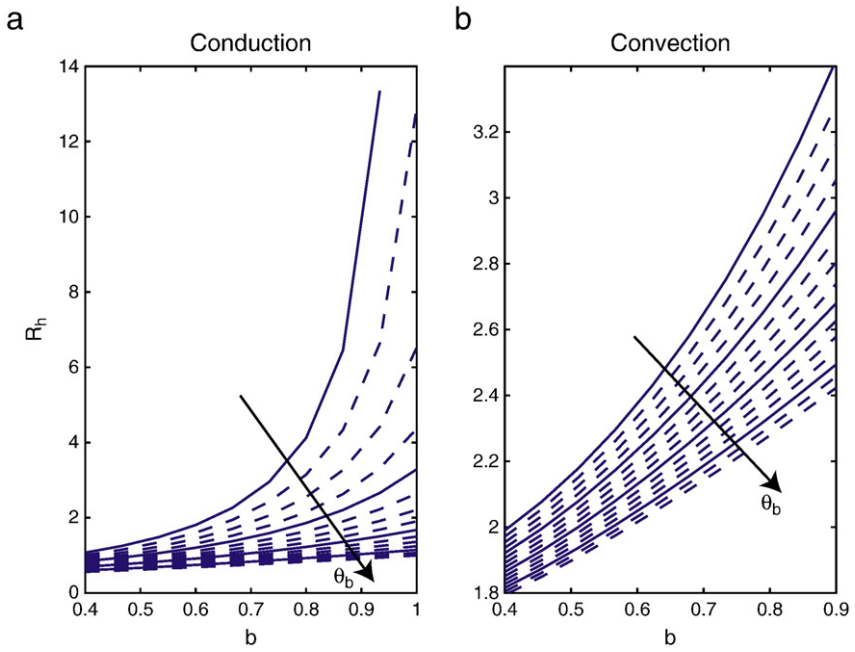

Fig. 6. Thickness of intrusion required for melting normalized by the thickness of the mush for a locking point crystallinity of 0.5, assuming that all the heat lost by the intrusion is transferred to the mush only.

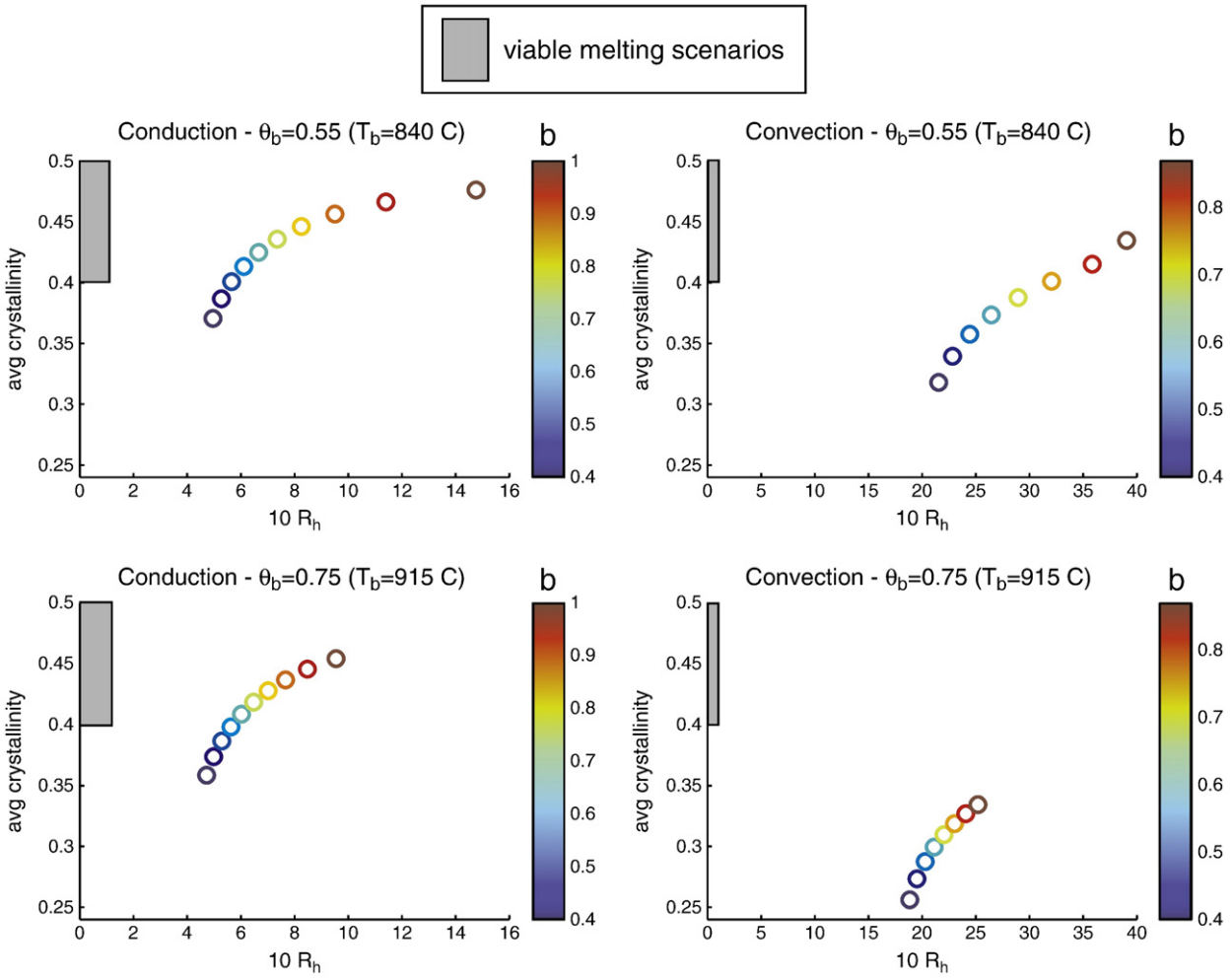

Fig. 7. Comparison of our results in terms of energy efficiency (here 10 times the thickness ratio $\mathcal{H}/H$) and average crystallinity for different power-law exponents b and viable melting scenarios satisfying the crystallinity constraint and where the intrusion size does not exceed the size of the mush. We compare results for two different intrusion–mush temperatures θ_b and both conduction and convection.

only. Using a 10% efficiency leads to intrusion sizes with an order of magnitude greater than the ones we calculated (i.e. intrusion thicker than the mush by about an order of magnitude). In all cases, even extreme intrusion fluxes over the existence of the mush will not be able to thermally reactivate midsize to large crystal mushes.

Optimal melting scenarios have to (1) satisfy the 40–50% average crystallinity constraint and (2) be sufficiently efficient energetically, which requires, at most, the emplacement of a volume of underplating magma of comparable size with the mush. Fig. 7 summarizes the results of our calculations for a range of mush temperature–crystallinity relationships and two different intrusion–mush temperature boundary conditions from both conduction and steady convection models. We fixed the thermal efficiency (fraction of heat loss by intrusion that is absorbed by the overlying mush) to 10% in agreement with thermal calculations. The results of our calculations are represented by open dots with a color-coding depending on the value of the power-law exponent b. The region of the plots that satisfies the average crystallinity and energy constraints is shaded. We arbitrarily choose the upper bound of the shaded area for $10R_h$ to be 1 for plausible thermal reactivation scenarios, as it represents a maximum thickness of intrusion comparable to the mush. This upper bound can be expanded to slightly higher values of $10R_h$ for small mushes. We observe that, over the range of parameters explored in our calculations, no melting scenario comes even close to satisfying both constraints.

5. Conclusions

The existence of erupted crystal-rich ignimbrites that often show evidence of pre-eruptive rejuvenation is often attributed to thermal reactivation events of locked crystal mushes associated with the underplating of more mafic magma intrusions. Erupted crystal mushes typically have a crystallinity of 40 to 50%, which imposes a strong constraint on the dynamical process that reactivates these systems prior to eruptions. In this study we focus on testing the ability of different melting scenarios associated with intrusions of magma to satisfy this crystallinity constraint.

We present a 1D analytical thermal model that solves for the heat transfer and melting of crystalline mushes with various temperature–crystallinity relationships. The model solves for the temperature and crystallinity distribution of the mush at any time and especially when the entire mush is open to convection. The existence of analytical solutions limits the model to either purely conductive cases or a parameterization of the convective heat flux in terms of a stagnant-lid convection scalings. We show that for the range of crystallinity–temperature relationships expected in silicic mushes ($b \sim 0.4$–0.5), the average crystallinity in the mushes that have melted sufficiently to develop full-scale convection is significantly less than the crystallinities observed in the field. Moreover, the remarkable homogeneity of the eruptive products is consistent with a physical model that includes convection and our choice of average crystallinity as a measure for chamber reactivation.

Furthermore, the thermal energy input needed to reactivate these systems requires intrusions that are at least one order of magnitude more voluminous than the mush. This suggests that thermal reactivation of mushes by injection of new magma cannot be the unique process that leads to the reactivation of midsize and large crystal mushes. Another process, combined with melting, is therefore required. This additional process has to (1) be more energetically favorable than melting alone and (2) be able to reactivate the mush with a smaller reduction of crystallinity than melting alone.

Acknowledgements

We would like to thank Michael Manga for stimulating discussions. C.H. was supported by a Swiss postdoctoral fellowship PBSKP2-128477, O.B was supported by NSF-EAR grant 0809828 and J.D. was supported by NSF-EAR grant 0838200.

References

Bachmann, O., Dungan, M.A., 2002. Temperature-induced Al-zoning in hornblendes of the fish Canyon magma, Colorado. American Mineralogist 87, 1062–1076.
Bachmann, O., Dungan, M.A., Lipman, P.W., 2002. The Fish Canyon magma body, San Juan volcanic field, Colorado: rejuvenation and eruption of an upper crustal batholith. Journal of Petrology 43, 1469–1503.
Bachmann, O., Bergantz, G.W., 2004. On the origin of crystal-poor rhyolites: extracted from batholitic crystal mushes. Journal of Petrology 45, 1565–1582.
Bachmann, O., Bergantz, G.W., 2006. Gas percolation in upper-crustal silicic crystal mushes as a mechanism for upward heat advection and rejuvenation of near-solidus magma bodies, Colorado. J. Volcanol. Geotherm. Res. 149, 85–102.
Bachmann, O., Bergantz, G.W., 2008. Rhyolites and their source mushes across tectonic settings, Colorado. Journal of Petrology 49, 2277–2285.
Christiansen, E.R., 2005. Contrasting processes in silicic magma chambers: evidence from very large volume ignimbrites. Geological Magazine 6, 669–681.
Costa, F., 2008. Residence times of silicic magmas associated with calderas. In: Marti, J., Gottsmann, J. (Eds.), Development in Volcanology, 10. Elsevier, pp. 1–55.
Couch, S., Sparks, R.S.J., Carroll, M.R., 2001. Mineral disequilibrium in lavas explained by convective self-mixing in open magma chambers:. Nature 411, 1037–1039.
Davaille, A., Jaupart, C., 1993. Transient high-Rayleigh-number thermal convection with large viscosity variations. Journal of Fluid Mechanics 253, 141–166.
Dingwell, D.B., Bagdassarov, N.S., Bussod, J., Webb, S.L., 1993. Magma rheology. Short Handbook on Experiments at High Pressure and Applications to the Earth's Mantle: Mineral. Assoc. Canada, 21, pp. 131–196.
Dufek, J., Bergantz, G.W., 2005. Lower crustal magma genesis and preservation: a stochastic framework for the evaluation of basalt–crust interaction. Journal of Petrology 46, 2167–2195.
Feltham, D.L., and Worster, M.G., Similarity solution describing the melting of a mush: Journal of Crystal Growth, v.208, p. 746–756.
Folkes, C.B., de Silva, S.L., Wright, H.M., and Cas, R.A.F., in press, Geochemical homogeneity of a long-lived, large silicic system; evidence from the Cerro Galán caldera, NW Argentina: Bulletin of Volcanology.
Ghiorso, M.S., Sack, R.O., 1995. Chemical mass transfer in magmatic processes IV: a revised and internally consistent thermodynamic model for the interpolation and extrapolation of liquid–solid equilibria in magmatic systems at elevated temperatures and pressures. Contributions to Mineralogy and Petrology 119, 197–212.
Hildreth, W., 1981. Gradients in silicic magma chambers: implications for lithospheric magmatism. Journal of Geophysical research 86, 10153–10192.
Huber, C., Bachmann, O., Manga, M., 2009. Homogenization processes in silicic manga chambers by stirring and mushification (latent heat buffering). Earth and Planetary Science Letters 283, 38–47.
Huber, C., Bachmann, O., Manga, M., 2010. Two competing effects of volatiles on heat transfer in crystal-rich magmas: thermal insulation vs defrosting. Journal of Petrology vol. 51, 847–867.
Koyaguchi, T., Kaneko, K., 1999. A two-stage thermal evolution model of magmas in continental crust. Journal of Petrology 40, 241–254.
Koyaguchi, T., Kaneko, K., 2001. Thermal evolution of silicic magma chambers after basalt replenishment:. Transactions of the Royal Society of Edimburgh 91, 47–60.
Lindsay, J.M., Schmitt, A.K., Trumbull, R.B., de Silva, S.L., Emmermann, R., 2001. Magmatic evolution of the La Pacana caldera system, Central Andes, Chile: compositional variation of the two cogenetic, large-volume felsic ignimbrites. Journal of Petrology 42, 459–486.
Lipman, P.W., 2004. Geological Map of the Central San Juan Caldera cluster, Southwestern Colorado. USGS Open File reprt, p. 2799.
Maughan, L.L., Christiansen, E.H., Best, M.G., Gromme, C.S., Deino, A.L., Tingey, D.G., 2002. The Oligocene Lund Tuff, Great Basin, USA: a very large volume monotonous intermediate. Journal of Volcanology and Geothermal Research 113, 129–157.
Marsh, B.D., 1981. On the crystallinity, probability of occurence, and rheology of lava and magma:. Contribution to Mineralogy and Petrology 78, 85–98.
Petford, N., 2003. Rheology of granitic magmas during ascent and emplacement: Annual Reviews of Earth and Planetary Sciences 31, 399–427.
Ruprecht, P., Bergantz, G.W., Dufek, J., 2008. Modeling of gas-driven magmatic overturn: tracking of phenocryst dispersal and gathering during magma mixing. Geochem. Geophys. Geosyst 9 (7). doi:10.1029/2008GC002022.
Turcotte, D.L., Schubert, G., 2002. Geodynamics, 2nd Edition. Cambridge University Press.
Turner, S., Costa, F., 2007. Measuring timescales of magmatic evolution. Elements 3, 267–272.
Vigneresse, J.-L., Barbey, P., Cuney, M., 1996. Rheological transitions during partial melting and crystallization with application to felsic magma segregation and transfer. Journal of Petrology 37, 1579–1600.